Atomic adsorption on the (020) surface of α-Pu: A density functional study

Raymond Atta-Fynn and Asok K. Ray*
Physics Department, University of Texas at Arlington, Arlington, Texas 76019, USA
(Received 19 May 2007; revised manuscript received 6 November 2007; published 7 February 2008)

Adsorption of atomic carbon, nitrogen, and oxygen on the (020) surface of α-Pu has been investigated using the full-potential linearized augmented-plane-wave plus local basis method. The Perdew-Burke-Ernzerhof exchange-correlation functional is used and the surface is modeled by a four-layer periodic slab consisting of a total of 32 Pu atoms. Adsorption energies have been optimized with respect to the distance of the adatom from the Pu surface for four adsorption sites, namely, the onefold top, onefold hollow, twofold short-bridge, and the twofold long-bridge sites. To investigate the effects of spin-orbit coupling on the adsorption process, computations have been carried out at two theoretical levels, one at the scalar-relativistic level with no spin-orbit coupling (NSOC) and one at the fully relativistic level with spin-orbit coupling (SOC). The short-bridge site was the most stable adsorption site for C, with chemisorption energies of 5.880 and 6.038 eV at the NSOC and SOC levels of theory, respectively. The long-bridge site was the most stable adsorption site for N and O, with chemisorption energies at the NSOC and SOC levels of theory, respectively, being 5.806 and 6.067 eV for N and 7.155 and 7.362 eV for O. The respective distances of the C, N, and O adatoms from the surface for the most stable adsorption sites were found to be 1.32, 1.26, and 1.35 Å. Our results show that SOC adsorption energies are more stable than NSOC adsorption energies in the 0.14–0.32 eV range. The work function and net spin magnetic moments, respectively, increased and decreased in all cases upon chemisorption compared to the bare surface. The local density of states and difference charge densities have been used to analyze the interaction between the adatoms and the substrate.

DOI: 10.1103/PhysRevB.77.085105 PACS number(s): 71.20.−b, 68.35.−p, 71.27.+a, 68.43.−h

I. INTRODUCTION

Considerable theoretical efforts have been devoted in recent years to studying the electronic and geometric structures and related properties of surfaces to high accuracy. One of the many motivations for this burgeoning effort has been a desire to understand the detailed mechanisms that lead to surface corrosion in the presence of environmental gases; a problem that is not only scientifically and technologically challenging but also environmentally important. Such efforts are particularly important for systems like the actinides, for which experimental work is relatively difficult to perform due to material problems and toxicity. As is known, the actinides are characterized by a gradual filling of the $5f$-electron shell with the degree of localization increasing with the atomic number Z along the last series of the periodic table and the increasing prominence of relativistic effects.[1–6] The narrower $5f$ bands, with properties intermediate between those of localized $4f$ and delocalized $3d$ orbitals, near the Fermi level, compared to $4d$ and $5d$ bands in transition elements, is believed to be responsible for the exotic structure of the actinides at ambient condition.[7,8]

The manmade metal plutonium (Pu) is located at the boundary between the light actinides (Th–Np) consisting of delocalized $5f$ electrons and the heavy actinides (Am–Lw) consisting of localized $5f$ electrons.[9–14] Plutonium is arguably the most complex metallic element known to mankind and has attracted extraordinary scientific and technological interest because of its unique properties. At ambient pressure, Pu undergoes six crystallographic transformations between room temperature and its melting point at 914 K, with the atomic volume changing by as much as 25%. The chemically complex nature of Pu arises from the fact that it is at the boundary of itinerant and localized $5f$ electrons. However, the exact phase of the delocalization-localization transition is still not clearly understood.

The ground state of Pu, α-Pu, has been determined experimentally as a low-symmetry monoclinic structure having space group $P2_1/m$ with 16 atoms in the crystal unit cell.[15] α-Pu, which is the most dense phase of Pu, is hard and brittle but soft vibrationally, with a Debye temperature of $\sim$200 K.[16] The experimentally determined lattice parameters for the 16-atom crystal cell of α-Pu are $a=6.183$ Å, $b=4.822$ Å, $c=10.963$ Å, $\alpha=\gamma=90°$, and $\beta=101.79°$. The crystal structure is such that eight atoms are distinct and the remaining eight atoms are generated by applying inversion on the eight distinct atoms. The eight distinct coordinates, which are of the form $(x,1/4,z)$, are listed in Table I. It follows that the remaining eight atoms have coordinates $(-x,-1/4,-z)$. Also listed in Table I are the ranges of the bond (short and long) distances of each Pu from the neighboring atoms as well as the number of bonds. It can clearly be seen that the short bond lengths fall in the range 2.57–2.78 Å while the long bonds fall in the 3.19–3.71 Å range. Figure 1 shows a picture of the monoclinic α-Pu crystal with the eight distinct atomic positions shown as colored big spheres and their inverted images as small spheres.

As is known, a significant number of experimental and theoretical studies exist in the literature for the bulk electronic and geometric structures of α-Pu,[17–34] and it has been demonstrated convincingly that density functional theory predicts the equilibrium volume and cohesive energy quite accurately, and that the $5f$ electrons are primarily delocalized. However, the magnetic nature of α-Pu, in fact of all phases of Pu, continues to be a matter of considerable controversies. Experimental data, in general, predict the absence

 ©2008 The American Physical Society

TABLE I. Crystal structure of α-Pu. The experimentally measured lattice parameters are $a=6.183$ Å, $b=4.822$ Å, $c=10.963$ Å, $\alpha=\gamma=90°$, and $\beta=101.79°$ (Ref. 15). The eight distinct atomic positions (scaled by lattice constants) and their corresponding long and short bonds are listed below. The remaining eight atoms in the unit cell are related to the eight distinct atoms via inversion symmetry.

Pu atom	Coordinates	Short bonds		Long bonds	
		Range (Å)	No.	Range (Å)	No.
1	(0.345,1/4,0.162)	2.57–2.76	5	3.21–3.71	7
2	(0.767,1/4,0.168)	2.60–2.64	4	3.19–3.62	10
3	(0.128,1/4,0.340)	2.58–2.66	4	3.24–3.65	10
4	(0.657,1/4,0.457)	2.58–2.74	4	3.26–3.42	10
5	(0.025,1/4,0.618)	2.58–2.72	4	3.24–3.51	10
6	(0.473,1/4,0.653)	2.64–2.74	4	3.21–3.65	10
7	(0.328,1/4,0.926)	2.57–2.78	4	3.30–3.51	10
8	(0.869,1/4,0.894)	2.76–2.78	3	3.19–3.71	13

of magnetism and theoretical work, in general, predicts an antiferromagnetic state. For the sake of brevity, we mention only a few results published in the literature here. Lashley *et al.*,[31] on the basis of new experimental data and reviews of previous data, have indicated that none of the experiments provided any evidence for ordered or disordered magnetic moments (either static or dynamic) in plutonium at low temperatures, in either the α or δ phase. On the other hand, using the projector augmented wave method, Sadigh *et al.*[32] have found the antiferromagnetic (AFM) configuration to have lower total energy than the nonmagnetic state. These calculations were performed with no spin-orbit (NSO) coupling. Using the full-potential linearized augmented-plane-wave (FPLAPW) method at the non-spin-polarized (NSP) SO and AFM SO levels only, Robert *et al.*[33] found that AFM generalized gradient approximation (GGA) calculations produced the α phase as the most stable structure of Pu. Employing the fully relativistic full-potential spin-polarized linearized augmented-plane-wave method, Kutepov and Kutepova[34] found that the nonmagnetic state of α-Pu has the highest total energy among the nonmagnetic, ferromagnetic, and antiferromagnetic states, while the anti-ferromagnetic state is the ground state with the lowest total energy. It is worth noting that these calculations did not include spin-orbit interaction. A very recent study by Shorikov *et al.*,[22] using the local density approximation with on-site Coulomb repulsion U and spin-orbit coupling (LDA+U+SO), found that the metallic Pu in both α and δ phases is nonmagnetic with Pu ions in f^6 configuration with zero values of spin, orbital, and total moments. Recently, Gong and Ray[35] have studied α-Pu at eight different theoretical levels (non-spin-polarized, spin-polarized, type-1 antiferromagnetic, type-2 antiferromagnetic, with each configuration considered without and with spin-orbit interaction) using the suite of software WIEN2K, and found the ground state to be antiferromagnetic (type-1 and type-2 energies were nearly degenerate). Thus, as stated earlier, the magnetic nature of the ground state of Pu, namely, that of α-Pu, remains controversial. Nevertheless, it is widely believed, at least in the theoretical community, that it is antiferromagnetic. Certainly further research, both experimental and theoretical, needs to be carried out to understand this perplexing discrepancy. We also hasten to point out that, to the best of our knowledge, no *ab initio* study has been reported in the literature for the surfaces of α-Pu or on atomic and molecular adsorption on such surfaces, though this is the ambient phase of Pu. Obviously, this is related to the highly complex electronic structure of α-Pu and the lack of any significant experimental data. In this study, we report theoretical *ab initio* electronic structure studies of adsorptions on α-Pu surfaces. In particular, we have studied the electronic structure of C, N, and O adsorbed on the (020) surface of α-Pu at select adsorption sites and compared, where appropriate, with our previously published results on C, N, and O chemisorption on the (001) and (111) surfaces of δ-Pu using the same computational method.[36]

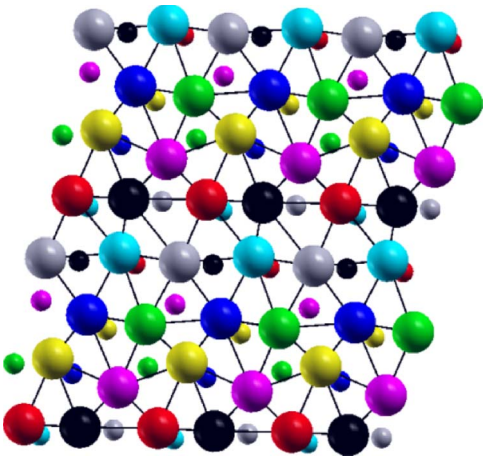

FIG. 1. (Color online) α-Pu crystal structure (Ref. 11).

II. COMPUTATIONAL METHODOLOGY

As in our previous work, all calculations have been performed within the generalized gradient approximation to density functional theory with the Perdew-Burke-Ernzerhof exchange-correlation functional.[37] The Kohn-Sham equa-

tions were solved using the all-electron full-potential linearized augmented-plane-wave plus local orbital (FP/LAPW+lo) basis method as implemented in the WIEN2K code.[38] This method makes no shape approximation to the potential or the electron density. Within the FP/LAPW+lo method, the unit cell is divided into nonoverlapping muffin tin spheres and an interstitial region. Inside the muffin tin sphere, the wave functions are expanded using radial functions (solution to the radial Schrödinger equation) times the spherical harmonics and in the interstitial region, the wave functions are expanded using plane waves. Madsen and co-workers[39] have demonstrated that using a hybrid basis set of LAPW/APW+lo for different angular momentum l of radial functions centered on the same atom yields a particularly accurate and efficient description. For our work, we have used the APW+LO basis to describe all s, p, d, and f ($l=0,1,2,3$) states and LAPW basis to describe all higher-angular-momentum states up to $l_{\mathrm{wf}}^{\mathrm{max}}=10$ in the expansion of the wave functions. Additional local orbitals were added to the $6s$ and $6p$ semicore states of Pu and $2p$ semicore states of C, N, and O to improve their description. The muffin tin radii have been chosen to be 2.15 bohr for Pu and 1.2 bohr for C, N, and O. Convergence tests yielded a plane-wave cutoff of 15.63 Ry (this corresponds to $R_{\mathrm{MT}}K_{\mathrm{max}}=8.5$ for the bare Pu slab and $R_{\mathrm{MT}}K_{\mathrm{max}}=4.7442$ for the Pu slab with adatom) and a k-point mesh of $5\times3\times1$ (with a temperature broadening parameter of $k_BT=0.005$ Ry for the Fermi surface) for the Brillouin zone integration. This broadening scheme avoids the instability originating from level crossings in the vicinity of the Fermi surface in metallic systems and also reduces the number of k points necessary to calculate the total energy of metallic systems.[40] Calculations were done both at the scalar relativistic [with no spin-orbit coupling (NSOC)] and at the fully relativistic [with spin-orbit coupling (SOC)] levels. Spin-orbit interactions are included via a second variational step using the scalar relativistic eigenstates as basis, where all eigenstates with energies below 4.5 Ry are included.[41] Furthermore, relativistic $p_{1/2}$ orbitals have been included to account for the finite character of the $p_{1/2}$ wave function at the nucleus.[42] In the literature, the electronic configuration of Pu is taken to be $[\mathrm{Rn}]5f^67s^2$ or $[\mathrm{Rn}]5f^56d^17s^2$, since the $5f$ and $6d$ energy levels are nearly degenerate. In WIEN2K, the ground-state configuration corresponds to the latter. The quantization axis for the SOC calculations was [001]. Self-consistency is achieved when total energies are converged to within 0.05 mRy or better. For α-Pu, an antiferromagnetic configuration of spins consisting of alternating spin-up and spin-down ferromagnetic sheets along the c axis has been used. To compute the adsorption energy, the positions of the Pu atoms are kept fixed at the experimental bulk lattice positions and only the distance of the adatom from the top layer is varied to yield the minimum energy. This is primarily for computational reasons because of the extremely computer-intensive nature of the calculations and also because it is believed that any possible relaxations and/or reconstructions of the α-Pu surface would be rather insignificant. Thus we do not believe that there will be any significant changes in the qualitative and quantitative conclusions of this study with inclusions of surface relaxations and/or reconstructions. We test this hypothesis further in the results to follow, specifically for oxygen atom adsorption.

As far as the specific α-Pu surface is concerned, x-ray diffraction studies clearly indicate that the observed intensities for the (211) and (020) surfaces of α-Pu are exceptionally strong.[15] However, the (020) orientation is the only atomically flat surface of α-Pu, and we have used this surface to study atomic adsorptions. From Table I, we note that the smallest surface unit cell for the (020) orientation contains eight distinct atoms and has dimensions $a=6.183$ Å, $b=10.963$ Å, and $\gamma=101.79°$, where the planar coordinates are given by the x and z coordinates in Table I. The stacking of the atomic layers in the (020) orientation will be of the form $ABAB\ldots$, where A corresponds to atoms with planar coordinates (x,z) (see Table I) and B corresponds to atoms with planar coordinates $(-x,-z)$, with the interlayer separation being 2.411 Å. The surface calculations have been performed with a slab geometry consisting of four atomic layers separated by a vacuum region of 15.9 Å (30 bohr) thickness. It follows that the four-layer slab plus vacuum will have dimensions $a=6.183$ Å, $b=10.963$ Å, $c=23.133$ Å with $\alpha=\beta=90°$ and $\gamma=101.79°$. We have previously shown for δ-Pu and fcc Am that a three-layer film is sufficient for studies of chemisorption[43] and we expect that for α-Pu, a four-layer film may indeed be sufficient.

In Fig. 2, the four-layer, 32-Pu-atom slab with an adatom at each of the four adsorption sites is shown. The second and third layers are related by inversion symmetry (atoms are colored red) and so are the first and fourth layers (colored gold). To preserve inversion symmetry, adatoms are adsorbed from both sides of the slab. The adsorption sites are the onefold top, onefold hollow, twofold short-bridge, and twofold long-bridge sites. At the top site the adatom sits directly on top of a Pu atom. At the hollow site the adatom is on top of a Pu atom on the second layer. At the short-bridge site, the adatom is between two Pu atoms having a short bond (see Table I), whereas, at the long-bridge site, the adatom is between two Pu atoms with a long bond. It worth noting that the surface unit cell looks like a distorted hexagonal layer and has virtually no symmetry. The lack of symmetry on the surface implies that several distinct adsorption sites of the same kind exist. Specifically, there are eight distinct top adsorption sites, eight distinct hollow adsorption sites, 16 distinct short-bridge sites, and 40 distinct long-bridge sites. For our calculations, a single adsorption site of a given type was considered, that is, one top site, one hollow site, one short-bridge site, and one long-bridge site were considered. We believe that adsorption energies at different sites of the same type will not differ significantly, that is, by not more than 0.1 eV. To confirm our assertion, as a test case, we chose a second top site for O adsorption and the difference in adsorption energies between the two sites was found to be 0.085 eV. The adsorption energy E_{ads} is calculated from

$$E_{\mathrm{ads}}=\frac{1}{2}[E(\text{bare Pu slab})+2E(\text{isolated adatom})-E(\text{Pu slab with adatom})], \quad (1)$$

with E being the total energy of the system in parentheses and a positive E_{ads} implying chemisorption. To compute the total energy of the isolated adatom, the adatom was simu-

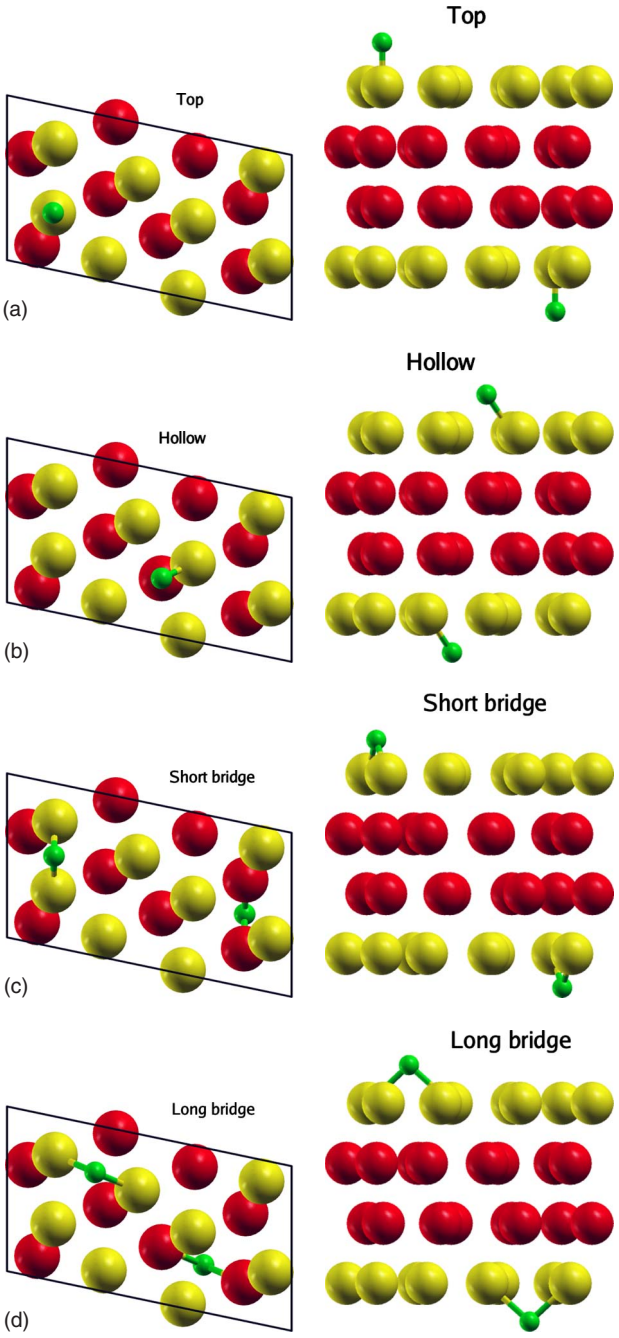

FIG. 2. (Color online) Top view (left) and side view (right) of adsorption sites on the α-Pu(020) surface. (a) Top; (b) hollow; (c) short bridge; (d) long bridge.

lated in a 25 bohr box and at the Γ point, under the same set of computational conditions.

Recently, we have studied, in great detail, the effects of spin-orbit coupling on the slab-adatom geometry and the adsorption energies for C, N, and O adsorbed on the (111) surface of δ-Pu.[36] We noted that the inclusion of spin-orbit interaction in the scalar relativistic Hamiltonian does not alter the adsorption geometry but the binding was slightly stronger with the chemisorption energies increasing by 0.05–0.3 eV. Though we have not verified it explicitly, we expect the same result to hold for the α-Pu surface. Hence in the current calculations, the geometry was optimized at the NSOC level and the final geometry was used for the SOC calculation so as to study spin-orbit coupling effects on the adsorption energies.

III. RESULTS AND DISCUSSIONS

Table II lists the adsorption energies and associated geometrical information of the C, N, and O atoms adsorbed on the (020) surface of α-Pu. The differences between the NSOC and SOC chemisorption energies at each adsorption site, given by $\Delta E_{\mathrm{ads}}=E_{\mathrm{ads}}^{\mathrm{SOC}}-E_{\mathrm{ads}}^{\mathrm{NSOC}}$, are also listed. For C adsorption, the chemisorption energies at the NSOC level of theory and the SOC case do not exhibit the same trend. At the NSOC level, the most stable site is the short-bridge site with a chemisorption energy of 5.880 eV, closely followed by the hollow site with a chemisorption energy of 5.772 eV, followed by the long-bridge site with chemisorption energy of 5.711 eV, with the least favorable site being the top site with chemisorption energy of 4.745 eV. At the SOC level, the most stable site is again the short-bridge site with a chemisorption energy of 6.038, but it is closely followed by the long-bridge site with a chemisorption energy of 6.031 eV, followed by the hollow site with a chemisorption energy of 6.021 eV, with the least favorable site again being the top site with a chemisorption energy of 4.997 eV. The vertical height z of the C adatom above the top layer is 1.89, 1.57, 1.66, and 1.32 Å for the top, hollow, short-bridge, and long-bridge sites, respectively. From our recent calculations on C adsorption on the (100) and (111) surfaces of δ-Pu,[36] we have found that increasing stability implies decreasing vertical distance of the C adatom from the surface layer. Also, increasing adatom coordination number implies increasing stability at both theoretical levels. Clearly, the previous observations do not hold here as, for instance, the one-fold hollow site at which the C adatom is further away from the surface binds more strongly than the twofold long-bridge site at which the adatom is closer to the surface. Also, we observed in our previous work[36] that increasing stability implies increasing Pu-C bond distances. This is also not observed here. One obvious reason is the lack of symmetry of the α-Pu(020) surface, which implies that, unlike on the δ-Pu surfaces, the adatoms on the α-Pu surface are not in a uniform bond environment (in the sense of bond distances, bond angles, etc.). However, as expected, all chemisorption energies in the SOC case are more stable than the NSOC case. ΔE_{C} is maximum at the long-bridge site (0.320 eV), followed by the least stable top site (0.252 eV), with the intermediately stable hollow site having $\Delta E_{\mathrm{C}}=0.249$ eV. The most stable short-bridge site has the smallest energy difference of 0.158 eV.

For N chemisorption, the most preferred site at the NSOC level of theory is the long bridge with a chemisorption energy of 5.806 eV. This is followed by the hollow and short-bridge sites with nearly degenerate chemisorption energies of 5.738 and 5.735 eV, respectively. The least preferred top site has a chemisorption energy of 4.950 eV. At the SOC level of theory, the most preferred site is the long-bridge site with a chemisorption energy of 6.067 eV, followed by the short-

TABLE II. Distances and chemisorption energies of C, N, and O on α-Pu(020). z is the distance of the adatom from the surface layer, $d_{\text{Pu-adatom}}$ is the Pu-adatom bond distance, $E_{\text{ads}}^{\text{NSOC}}$ and $E_{\text{ads}}^{\text{SOC}}$ are the chemisorption energies at the NSOC and SOC levels of theory, and $\Delta E_{\text{ads}}=E_{\text{ads}}^{\text{SOC}}-E_{\text{ads}}^{\text{NSOC}}$ is the difference between the SOC and NSOC chemisorption energies at each adsorption site. The numbers in parentheses denote results for O adsorption on the fully relaxed slab.

Adatom	Site	z (Å)	$d_{\text{Pu-adatom}}$ (Å)	$E_{\text{ads}}^{\text{NSOC}}$ (eV)	$E_{\text{ads}}^{\text{SOC}}$ (eV)	ΔE_{ads} (eV)
Carbon	Top	1.89	1.89	4.745	4.997	0.252
	Hollow	1.57	1.90	5.772	6.021	0.249
	Short bridge	1.66	2.10	5.880	6.038	0.158
	Long bridge	1.32	2.07	5.711	6.031	0.320
Nitrogen	Top	1.83	1.83	4.950	5.167	0.217
	Hollow	1.51	1.85	5.738	5.882	0.144
	Short bridge	1.59	2.05	5.735	5.900	0.165
	Long bridge	1.26	2.03	5.806	6.067	0.261
Oxygen	Top	1.88 (1.88)	1.88 (1.88)	6.645 (6.670)	6.822 (6.624)	0.177
	Hollow	1.59 (1.61)	1.92 (1.92)	7.034 (7.015)	7.230 (7.102)	0.196
	Short bridge	1.68 (1.69)	2.12 (2.12)	7.021 (6.969)	7.167 (6.941)	0.146
	Long bridge	1.35 (1.40)	2.09 (2.10)	7.155 (7.058)	7.362 (7.255)	0.207

bridge and hollow sites with basically degenerate chemisorption energies of 5.900 and 5.882 eV, respectively. Again the top site is the least favorable site with a chemisorption energy of 5.167 eV. The optimum heights of the adatom above the surface are found to be 1.83, 1.51, 1.59, and 1.26 Å for the top, hollow, short-bridge, and long-bridge sites, respectively. As noted for C adsorption, we note here also that no well-defined relationship exists between adsorption site coordination number and chemisorption energies. The SOC-NSOC chemisorption energy differences listed in Table II show that SOC chemisorption energies are more stable than NSOC energies in the 0.144–0.261 eV range.

The trend in the chemisorption energies at the NSOC level of theory is the same as that in the SOC case for O adsorption. The most stable site is the long-bridge site (7.155 eV for the NSOC case, 7.362 eV for the SOC case), closely followed by the hollow site (7.034 eV for the NSOC case, 7.230 eV for the SOC case), and the short-bridge site (7.021 eV for the NSOC case, 7.167 eV for the SOC case). The least favorable site is the top site (6.645 eV for the NSOC case, 6.822 eV in the SOC case). The heights of the adatom above the surface are 1.88, 1.59, 1.68, and 1.35 Å for the top, hollow, short-bridge, and long-bridge sites, respectively. Here, however, the relationships z(long bridge) $<z$(hollow) $<z$(short bridge) $<z$(top) and E_{ads}(long bridge) $>E_{\text{ads}}$(hollow) $>E_{\text{ads}}$(short bridge) $>E_{\text{ads}}$(top) are found to be true and have been observed, in general, for equivalent sites in the case of O adsorption on the (100) and (111) surfaces of δ-Pu.[36]

As mentioned before, Sadigh *et al.*[32] studied relaxation effects in bulk α-Pu extensively and observed that the amount of relaxation was quite small. To verify the effects, if any, of relaxation on the adsorption process, we first optimized the atomic volume of the bulk monoclinic unit cell subject to the constraints that the ratios of the lattice constants b/a and c/a, as well as the angles between the lattice vectors α, β, and γ, were fixed at the experimental values. The optimized atomic volume of bulk α-Pu was 126.7 bohr^3, which is a contraction of 6.08% of the experimental atomic volume of 134.9 bohr^3.[15] In the next step, the resulting lattice parameters were used to construct the four-layer slab. The slab has three interlayer separations d_{12} (between the top and second layers), d_{23} (between the second and third layers), and d_{34} (between the third and bottom layers). We note that $d_{12}=d_{34}$ due to inversion symmetry. The minimization of the slab total energy with respect to d_{12} and d_{23} was performed by computing the total energy for several variations of d_{12} and d_{23} and generating a surface. The expansion or contraction of the interlayer separation with respect to the bulk interlayer spacing d_0 is given by $\Delta d_{ij}=100(d_{ij}-d_0)/d_0$. Figure 3 depicts the surface plot of the total energy (shifted by +1 900 289 Ry) as a function of Δd_{12} and Δd_{23}. Both layers contracted, with the interlayer relaxation corresponding to the minimum energy being $\Delta d_{12}=-4.4\%$ and $\Delta d_{23}=-5.4\%$. Furthermore, relaxation lowered the total energy of the slab by 1.26 mRy/atom compared to the slab at the bulk geom-

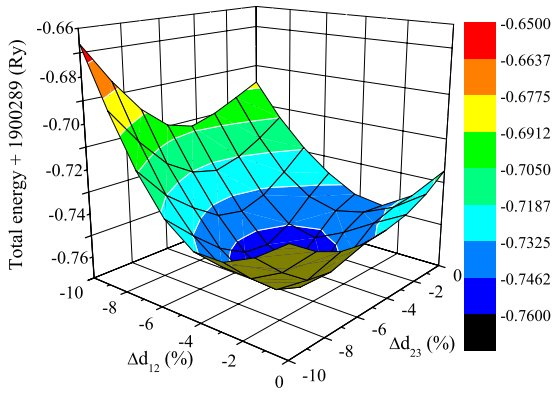

FIG. 3. (Color online) Relaxation of α-Pu(020) four-layer slab. $\Delta d_{ij}=100(d_0-d_{ij})/d_0$, where d_{ij} is the separation between layers i and j and d_0 is the bulk interlayer separation.

etry. We then studied the adsorption of the oxygen atom, which is the most reactive among the three adsorbates, on the fully relaxed surface. These results, along with the results for O adsorption on the nonrelaxed slab, are also reported in Table II. The chemisorption energies and the distances from the surface corresponding to adsorption on the relaxed slab are shown in parentheses. First of all, the relative ordering of the stability with respect to the chemisorption energies is preserved for both the relaxed and nonrelaxed cases at each theoretical level, that is, long bridge>hollow>short bridge >top. For adsorption on the relaxed slab, the most stable site is the long-bridge site (7.058 eV for the NSOC case, 7.255 eV for the SOC case), followed by the hollow site (7.015 eV for the NSOC case, 7.102 eV for the SOC case), then the short-bridge site (6.969 eV for the NSOC case, 6.941 eV for the SOC case), with the top site again having the least favorable binding energy (6.670 eV for the NSOC case, 6.624 eV for the SOC case). The percentage differences from the corresponding values for the nonrelaxed slab are 1.36, 0.27, 0.74, and 0.38, respectively for the NSOC case. The values for the SOC case are 1.46, 1.79, 3.20, and 2.95, respectively. In general, the binding energies corresponding to adsorption on the nonrelaxed slab are slightly more stable but the variations in energy differences from site to site are somewhat preserved in the two cases. The optimized heights of the adatom above the surface for the relaxed slab are 1.88, 1.61, 1.69, and 1.40 Å for the top, hollow, short-bridge, and long-bridge sites respectively, the percentage differences from the corresponding values of the nonrelaxed slab being 0.0, 1.25, 0.59, and 3.64, respectively, indicating nonsignificant variations of adsorption geometries between the nonrelaxed and the fully relaxed slabs. Since the chemisorption energies and distances for adsorption on the nonrelaxed and relaxed slabs show very little departure from each other, it is plausible to conclude that the effects of relaxation are small. We expect this conclusion will hold true for carbon and nitrogen. Also it should be noted here that the relationships $z(\text{long bridge}) < z(\text{hollow}) < z(\text{short bridge}) < z(\text{top})$ and $E_{\text{ads}}(\text{long bridge}) > E_{\text{ads}}(\text{hollow}) > E_{\text{ads}}(\text{short bridge}) > E_{\text{ads}}(\text{top})$ hold true for the relaxed surface also. All discussions that follow pertain to the nonrelaxed slab.

In Table III, the adsorbate-induced work function changes with respect to the clean metal surface, given by $\Delta\Phi = \Phi^{\text{adatom/Pu}} - \Phi^{\text{Pu}}$, where Φ^{Pu} and $\Phi^{\text{adatom/Pu}}$ are, respectively, the work functions of the clean metal surface and the metal surface with adatom are listed for the NSOC and SOC levels of theory for each adsorbate and each adsorption site. We obtained $\Phi^{\text{Pu}}=3.51$ and 3.62 eV at the NSOC and SOC theoretical levels. On the other hand, for the δ-Pu(111) surface, the most stable surface of δ-Pu, the work functions are 3.26 and 3.49 eV at the NSOC and SOC levels of theory, respectively. We observe for each adatom and each theoretical level that high chemisorption energies usually correspond to low work function shifts. In general, the changes in the work functions are largest at the least preferred top sites and lowest at the most preferred hollow sites. The trends in the work function agree well with recent adsorption calculations on δ-Pu surfaces.[36] The work function shifts can be understood in terms of the surface dipoles arising due to the partial transfer of electrons from the Pu surface to the adsorbates since the electronegativities of all the adatoms are larger than that of Pu. The surface dipole moment μ (in debyes) and the work function shift $\Delta\Phi$ (in eV) are linearly related by the Helmholtz equation $\Delta\Phi = 12\Pi\Theta\mu/A$, where A is the area in Å^2 per (1×1) surface unit cell and Θ is the adsorbate coverage in monolayers.[44] However, considering the top and bridge sites, which are common to both the δ-Pu and α-Pu surfaces, the magnitudes of the adsorbate-induced work function shifts for δ-Pu are on the average 0.5 eV greater than those of α-Pu.[36]

TABLE III. Change in work function $\Delta\Phi = \Phi^{\text{adatom/Pu}} - \Phi^{\text{Pu}}$ (in eV) for both the NSOC and SOC levels of theory. $\Phi^{\text{Pu}}=3.51$ and 3.62 eV, respectively, at the NSOC and SOC theoretical levels.

Theory	Site	Carbon	Nitrogen	Oxygen
NSOC	Top	0.71	0.52	0.43
	Hollow	0.51	0.42	0.32
	Short bridge	0.37	0.41	0.36
	Long bridge	0.51	0.24	0.30
SOC	Top	0.67	0.57	0.45
	Hollow	0.56	0.39	0.29
	Short bridge	0.57	0.41	0.32
	Long bridge	0.40	0.27	0.19

In Table IV, the magnitude and alignment of the site-projected spin magnetic moments for each Pu atom on each atomic layer, as well as the net spin magnetic moment per Pu atom at the SOC theoretical level, are reported for the clean metal surface and the chemisorbed systems. The NSOC moments follow a similar qualitative and quantitative trend and are not reported here. Here S_i are the spin moments inside the muffin tin for the ith Pu atom in each layer; S_{int} and S_{tot} are, respectively, the interstitial spin moment and net moment per Pu atom, respectively. The spin moments of Pu atoms bonded to the adatoms are printed in bold. Looking at the spin moments for the bare slab, it is clearly evident that the final spin configuration is not totally antiferromagnetic. Also, the magnitudes of the spin moments of the surface atoms are in general larger than the spin moments of the atoms on the subsurface. For the onefold top sites, we note sufficiently large reductions (more than $2.45\mu_B$) in the spin moment of the Pu atom bonded to the adatom while the moments for the remaining atoms remain primarily unaltered compared to the clean metal. This leads to a reduction in the net spin magnetic moment per Pu atom. The same scenario can be observed for the onefold hollow site, where the reduction of the spin moment of the Pu atom bonded to the adatom is about $2.0\mu_B$. For the twofold bridge sites, we see a reduction of about $0.41\mu_B - 2.26\mu_B$ in the spin moments of the two surface layer Pu atoms interacting with the adatom, since the adatom sits exactly between the two Pu atoms, leading to a reduction in the net spin magnetic moments. Reduction of the spin magnetic moments as a result of chemisorption has also been observed for C, N, and O adsorption on the (111) and (100) surfaces of δ-Pu.[36]

Due to the nature of the APW+lo basis, the electronic charges inside the muffin tin spheres can be decomposed into

TABLE IV. Spin magnetic moments S_i for the Pu atoms on each layer for the fully relativistic calculation. Layer 1 is the surface layer and layer 2 is the subsurface layer. Layer 4 (layer 3) is related to layer 1 (layer 2) via inversion symmetry, and hence they have the same spin moments. The interstitial spin magnetic moment S_{int} and net spin magnetic moment are also given. Spin moments in bold type denote Pu atoms bonded to the adatoms.

System	Site	Layer	Spin magnetic moment (μ_B)									S_{tot} (μ_B/Pu)
			S_1	S_2	S_3	S_4	S_5	S_6	S_7	S_8	S_{int}	
Bare slab		1	−2.78	−1.32	−2.78	−2.94	−3.31	−3.06	−4.03	−3.19	−6.72	−0.99
		2	1.82	3.37	1.33	1.76	1.43	1.35	−1.49	1.36		
C	Top	1	**0.11**	−1.73	−2.91	−3.01	−3.33	−3.09	−4.02	−3.30	−5.72	−0.86
		2	1.37	3.36	1.18	1.70	1.42	1.31	−1.45	1.42		
	Hollow	1	−2.89	−1.38	−2.80	−2.91	−3.23	−2.94	−3.97	**−0.35**	−4.81	−0.77
		2	2.05	3.34	1.35	1.66	1.47	1.66	−1.68	0.64		
	Short bridge	1	**−2.02**	**−0.15**	−2.90	−3.00	−3.34	−3.11	−4.04	−3.33	−5.71	−0.84
		2	1.50	3.32	1.43	1.74	1.45	1.31	−0.99	1.46		
	Long bridge	1	**−0.52**	−1.72	−2.91	−2.98	−3.34	−3.09	**−3.33**	−3.25	−5.04	−0.79
		2	1.58	3.39	1.22	1.80	1.43	1.53	−1.62	1.67		
N	Top	1	**0.03**	−1.95	−2.97	−3.02	−3.32	−3.08	−4.04	−3.29	−5.98	−0.88
		2	1.17	3.36	1.31	1.77	1.41	1.32	−1.21	1.39		
	Hollow	1	−2.88	−1.72	−2.85	−2.98	−3.29	−3.02	−4.02	**−1.14**	−5.17	−0.78
		2	1.88	3.35	1.53	1.87	1.63	1.46	−0.94	1.12		
	Short bridge	1	**−1.94**	**−0.31**	−2.90	−3.01	−3.33	−3.10	−4.05	−3.36	−5.83	−0.85
		2	1.70	3.32	1.41	1.77	1.48	1.36	−1.36	1.53		
	Long bridge	1	**−0.81**	−1.54	−2.88	−2.98	−3.34	−3.09	**−3.37**	−3.26	−5.27	−0.82
		2	1.58	3.38	1.09	1.77	1.37	1.58	−1.72	1.70		
O	Top	1	**−0.31**	−1.98	−2.99	−3.01	−3.32	−3.08	−4.04	−3.29	−6.17	−0.92
		2	1.21	3.40	1.29	1.75	1.35	1.35	−1.47	1.45		
	Hollow	1	−2.86	−1.02	−2.79	−2.94	−3.27	−3.02	−4.05	**−1.14**	−5.10	−0.80
		2	2.11	3.37	1.26	1.63	1.44	1.64	−1.93	1.27		
	Short bridge	1	**−2.17**	**−0.78**	−2.83	−2.97	−3.29	−3.04	−4.05	−3.32	−6.09	−0.91
		2	1.64	3.29	1.36	1.71	1.41	1.22	−1.20	1.40		
	Long bridge	1	**−1.56**	−1.40	−2.84	−2.98	−3.33	−3.09	**−3.62**	−3.26	−5.56	−0.87
		2	1.81	3.37	1.11	1.76	1.36	1.61	−1.78	1.67		

contributions from the different angular momentum channels. We refer to these charges as partial charges. By comparing the partial charges Q_B of the Pu layers and adatoms before adsorption to the corresponding partial charges Q_A after adsorption, we get an idea of the nature of the interaction between the adsorbate and substrate. All adatoms exhibit the same trends and, as a generic example, we report Q_A and Q_B for oxygen and the Pu atoms in Table V. A relevant quantity that facilitates the discussion is the differential partial charge of a given state l corresponding to a given atom, which is given by $\Delta Q(l)=Q_A-Q_B$. $\Delta Q>0$ indicates charge gain inside the muffin tin sphere, while $\Delta Q<0$ indicates otherwise. It is immediately obvious from the table that ΔQ is very small ($0.01e$) or completely vanishes for the subsurface layer Pu atoms. This suggests that the Pu-adatom interaction is confined mainly to the surface layer. $\Delta Q(p)$ is in the $0.21e-0.24e$ range for the O adatom at the four adsorption sites, implying the displacement of electronic charges from the substrate toward the adatom. This is expected as the adatoms are more electronegative than the Pu atoms. Regarding the Pu atoms on the surface layer, it can clearly be seen that the values of ΔQ for the d and f states are generally quite significant for the Pu atoms interacting with the adatoms (with corresponding Q_A and Q_B indicated in bold), while very little change is observed for the remaining Pu atoms. For the Pu atom at the onefold top site, $\Delta Q(d)=0.11e$ and $\Delta Q(f)=-0.13e$; for the Pu atom at the onefold hollow site, $\Delta Q(d)=0.07e$ and $\Delta Q(f)=-0.09e$; for the two Pu atoms at the twofold short-bridge site, the combined differential charges are $\Delta Q(d)=-0.01e$ (which is quite small compared to the top and hollow sites) and $\Delta Q(f)=-0.08e$; for the two Pu atoms at the twofold long-bridge site, the combined differential charges are $\Delta Q(d)=0.05e$ and $\Delta Q(f)=-0.16e$. It can therefore be deduced, albeit not with complete certainty (as the electron density in the interstitial cannot be resolved), that significant O(p)-Pu(d)-Pu(f) interactions occur during adsorption. Similar observations hold for C and N.

To investigate the nature of the bonds that have been formed between the adatoms and the Pu atoms on the surface, we computed the difference charge density distribution

TABLE V. Partial charges inside the muffin tin spheres for Pu atoms (d,f) on each atomic layer and O adatom (p), where Q_A is the partial charge inside a muffin tin sphere after adsorption and Q_B is the partial charge inside a muffin tin sphere before adsorption. S denotes the surface layer and $S-1$ denotes the subsurface layer. Partial charges for the adatom and Pu atoms bonded to the adatom at a given site are indicated in bold font.

		Q_B			Q_A											
		Bare slab and isolated adatom			Top			Hollow			Short bridge			Long bridge		
		p	d	f	p	d	f	p	d	f	p	d	f	p	d	f
S	O	2.19			2.40			2.41			2.41			2.43		
	Pu1		0.61	4.46		**0.72**	**4.33**		0.61	4.46		**0.61**	**4.41**		**0.62**	**4.39**
	Pu2		0.69	4.44		0.67	4.47		0.68	4.45		**0.68**	**4.41**		0.68	4.45
	Pu3		0.62	4.44		0.60	4.47		0.62	4.44		0.61	4.46		0.62	4.45
	Pu4		0.61	4.43		0.61	4.44		0.61	4.44		0.61	4.44		0.61	4.43
	Pu5		0.58	4.44		0.58	4.44		0.57	4.46		0.58	4.44		0.58	4.44
	Pu6		0.59	4.44		0.59	4.45		0.58	4.46		0.60	4.44		0.59	4.45
	Pu7		0.47	4.49		0.47	4.50		0.45	4.51		0.47	4.49		**0.51**	**4.40**
	Pu8		0.59	4.45		0.59	4.46		**0.66**	**4.36**		0.57	4.48		0.58	4.48
$S-1$	Pu1		0.67	4.39		0.67	4.38		0.67	4.39		0.67	4.39		0.67	4.38
	Pu2		0.55	4.38		0.54	4.39		0.55	4.38		0.55	4.38		0.55	4.38
	Pu3		0.67	4.37		0.67	4.37		0.67	4.37		0.67	4.38		0.67	4.37
	Pu4		0.65	4.37		0.65	4.37		0.65	4.37		0.65	4.37		0.65	4.37
	Pu5		0.67	4.37		0.67	4.37		0.67	4.38		0.66	4.38		0.66	4.38
	Pu6		0.69	4.39		0.69	4.39		0.69	4.40		0.69	4.40		0.69	4.40
	Pu7		0.74	4.42		0.74	4.42		0.74	4.43		0.74	4.42		0.74	4.43
	Pu8		0.68	4.40		0.68	4.40		0.68	4.40		0.68	4.40		0.68	4.41

for the O chemisorbed system, since the O adatom interacts more strongly with the Pu surface. We define the difference charge density $\Delta n(r)$ as follows:

$$\Delta n(r) = n(\mathrm{O+Pu}) - n(\mathrm{Pu}) - n(\mathrm{O}),$$

where n(O+Pu) is the total electron charge density of the Pu slab with O adatom, n(Pu) is the total charge density of the bare Pu slab, and n(O) is the total charge density of the O adatom. In computing n(O) and n(Pu), the Pu and O atoms are kept fixed at exactly the same positions as they were in the chemisorbed systems. All densities reported here were computed in the plane passing through the adatom and two surface Pu atoms using the XCRYSDEN utility.[45] For the onefold-coordinated sites, the plane passes through the adatom, the Pu atom interacting with the adatom, and a neighboring Pu atom. For the twofold-coordinated sites, the plane passes through the adatom and the two Pu atoms interacting with the adatom. Figure 4 shows the difference charge density distribution for O adsorption for each site. For the top site, we clearly see charge accumulation around the O adatom and significant charge loss around the Pu atom on which the O atoms sits, implying that the bond has a strong ionic character, which is expected as the adatoms are more electronegative than the metal. We also see some charge accumulation around the Pu atom. Overall, this is fairly consistent with the differential partial charges inside the muffin tin sphere reported in Table V, where the O p states gain charge, the Pu d states gain charge, and the Pu f states lose charge. The plot for the onefold hollow site bears resemblance to that of the top site. For the bridge site, the significant charge accumulation around the O adatom is evident, with clear charge depletion around both Pu atoms as one moves from O to Pu along the Pu-O bonds. This again suggests that bonding is primarily ionic. The difference charge density distributions for C and N show the similar behavior and are not reported here.

We have also examined the local density of electron states (LDOS). This is obtained by decomposing the total density of the single-particle Kohn-Sham eigenstates into contributions from each angular momentum channel l of the constituent atoms inside the muffin tin sphere. We have reported the LDOS for only the SOC computation. In Fig. 5, the Gaussian-broadened (with a width of 0.045 eV) f and d LDOS curves for each of the layers of the clean α-Pu(020) metal slab as well as that of the bulk monoclinic unit cell are shown. Clearly, the well-defined peaks and valleys in the $5f$-electron LDOS in the vicinity of the Fermi level, which we have observed for pure δ-Pu metal or its surfaces,[36] are not observed here. In general, the $5f$ DOS at the Fermi level is small compared to that of δ-Pu. Also, the nature of the $5f$ bands at just below and above the Fermi level is quite broad which might indicate some $5f$-electron delocalization. We note that the $5f$ bands for the subsurface and the bulk have similar features below and above the Fermi level.

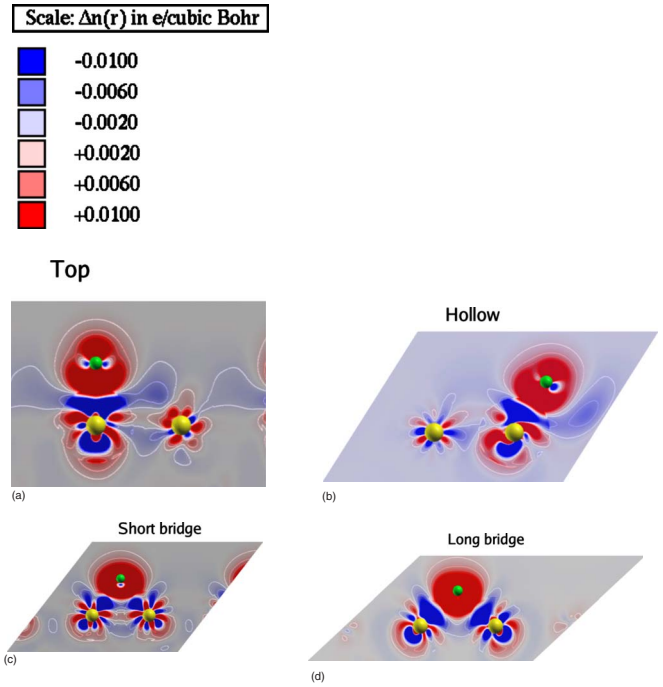

FIG. 4. (Color online) Difference charge density distributions $\Delta n(r)$ for O on α-Pu(020) surface. O atom is colored green and Pu atoms are colored gold. The scale used for coloring is shown at the top. Red (positive) denotes regions of charge accumulation and blue (negative) denotes regions of charge depletion. (a) Top; (b) hollow; (c) short bridge; (d) long bridge.

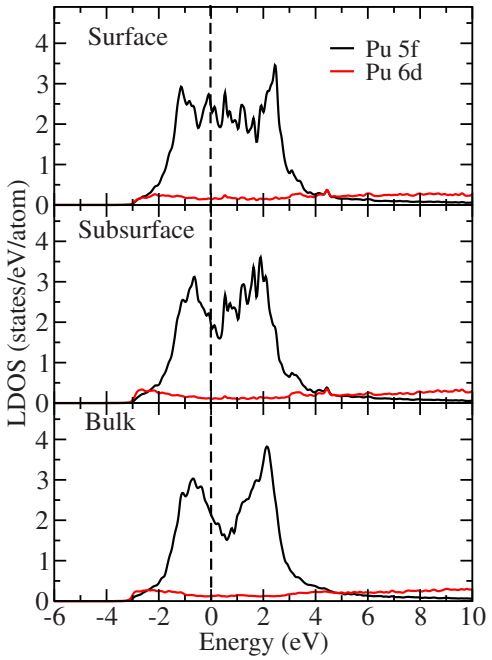

FIG. 5. (Color online) f and d LDOS plots for surface and subsurface layers of α-Pu(020) and the bulk monoclinic α-Pu unit cell. Vertical line through $E=0$ is the Fermi level. LDOS corresponds to calculations with SOC.

As there are several nonequivalent atoms on the surface, only the LDOS of the adatoms and the surface Pu atoms interacting with the adatoms are considered. In Fig. 6, we show the LDOS plots for the C adatom and the surface Pu atoms to which it is bonded. We note that the $5f$ DOS of the atom Pu1 on which the adatom sits is modified, with a reduction of the DOS at the Fermi level (in comparison to the surface layer LDOS for the clean Pu slab in Fig. 5), which implies that the $5f$ electrons participate in chemical bonding and therefore become further delocalized. We also observe complete Pu1($6d$)-Pu1($5f$)-C($2p$) overlaps. The LDOS distribution for the hollow site is similar to that of the top site. In comparison to the surface layer LDOS of the bare slab, we again observe a reduction in the $5f$ DOS at the Fermi level, indicating the participation of the $5f$ orbitals in bonding. Pu ($6d$)-Pu ($5f$)-C ($2p$) hybridization is also evident. The behavior of the LDOS plots for the short-bridge and long-bridge sites also shows significant hybridizations just like the ones observed for top and hollow sites.

In Fig. 7, the LDOS plots for N chemisorptions are shown. For the top site, we see a significant character of the $5f$ and $6d$ bands of Pu1 in the N $2p$ bands. This indicates significant Pu($6d$)-Pu($5f$)-N($2p$) hybridization. We must mention that the spurious peak at about 1 eV below the Fermi level, which we attribute mainly to numerical noise, is not, in our opinion, a sign of $5f$-electron localization ($5f$-electron localization has a well-defined signature). For the hollow site, Pu($6d$)-Pu ($5f$)-N ($2p$) overlap is clearly evident with a slight reduction in DOS at the Fermi level compared to the clean slab. The hybridization of the bands in LDOS plots for the short- and long-bridge sites is qualitatively similar to the plots for the top and hollow sites except that, at the long-bridge site, the N $2p$ bands move to slightly

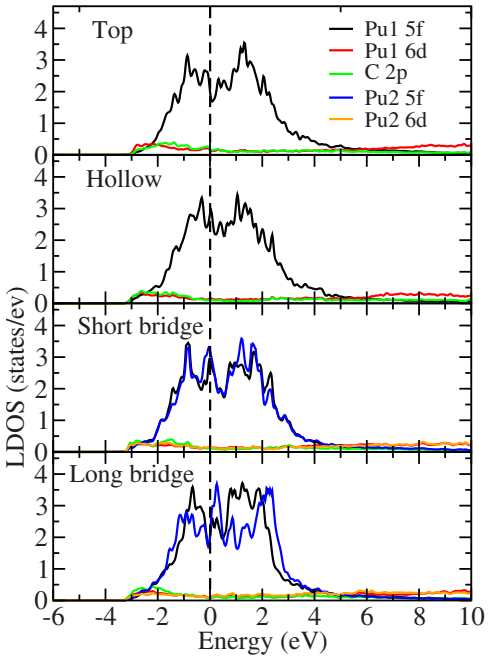

FIG. 6. (Color online) d and f LDOS curves inside the muffin tin for the Pu atoms on the surface layer and p LDOS curves for C adatom. Vertical line through $E=0$ is the Fermi level. LDOS corresponds to calculations with SOC.

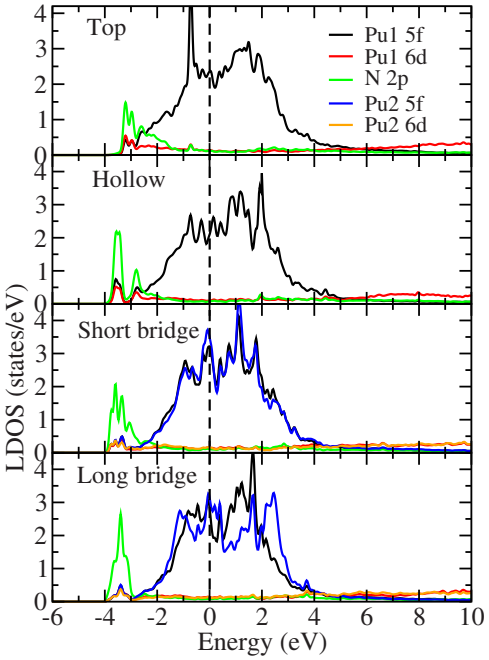

FIG. 7. (Color online) d and f LDOS curves inside the muffin tins for the Pu atoms on the surface layer and p LDOS curves for N adatom. Vertical line through $E=0$ is the Fermi level. LDOS corresponds to calculations with SOC.

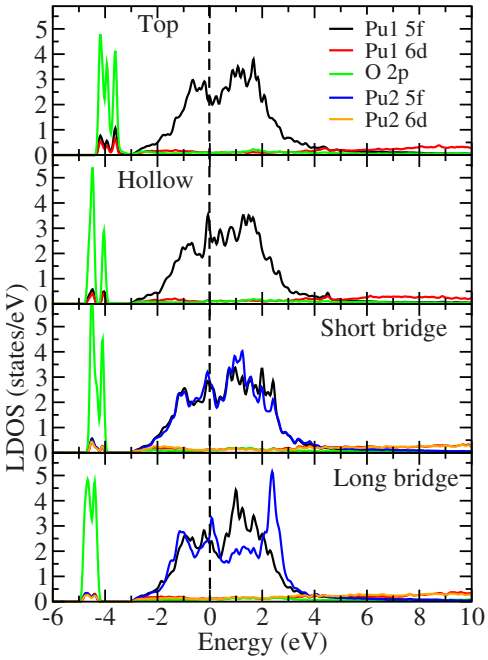

FIG. 8. (Color online) d and f LDOS curves inside the muffin tins for the Pu atoms on the surface layer and p LDOS curves for O adatom. Vertical line through $E=0$ is the Fermi level. LDOS corresponds to calculations with SOC.

lower energies, which is reflected in the high chemisorption energies.

In Fig. 8, we show the LDOS plots for O chemisorption. The behavior of the LDOS at each site is qualitatively similar to that of C and N. For the top site, the hybridizations of the eigenstates are evident, with a slight reduction in the $5f$ DOS of Pu1. For the remaining sites, we observe significant hybridizations between the $6d$ states of Pu and the $2p$ states of O with an admixture with Pu $5f$ states. We also observe that from the top to hollow to short-bridge to long-bridge sites, O $2p$ bonding states are gradually pushed to lower energies leading to stronger binding.

IV. CONCLUSIONS

In summary, we have used the generalized gradient approximation to density functional theory with the full potential LAPW+lo method to study chemisorption of C, N, and O atoms on the (020) surface of α-Pu at two theoretical levels; one with no spin-orbit coupling and the other with spin-orbit coupling. The top site was the least preferred site and a bridge (short or long) site was the most preferred site in all cases. The inclusion of spin-orbit coupling increases the chemisorption energies by 0.14–0.32 eV. Work functions increased in all cases compared to the clean Pu surface, with the largest shift corresponding to the least preferred top site and the lowest shifts corresponding to bridge sites in general. Upon adsorption, the net spin magnetic moment of the chemisorbed system decreases in each case compared to that of the bare surface. Difference charge density plots clearly show that the bonds between the surface Pu atom and the adatoms at each site are largely ionic in character. A study of the local density of states indicates that at the least favorable top site there is a reduction in the $5f$ DOS at the Fermi level of the Pu atom on top of which the adatoms sit, implying further delocalization of the $5f$ electrons upon chemisorption. Significant Pu ($6d$)-Pu ($5f$)-adatom ($2p$) hybridizations are also observed in all cases.

ACKNOWLEDGMENTS

This work is supported by the Chemical Sciences, Geosciences and Biosciences Division, Office of Basic Energy Sciences, Office of Science, U.S. Department of Energy (Grant No. DE-FG02-03ER15409) and the Welch Foundation, Houston, Texas (Grant No. Y-1525). In addition to the supercomputing facilities at the University of Texas at Arlington, this research also used resources of the National Energy Research Scientific Computing Center, which is supported by the Office of Science of the U.S. Department of Energy under Contract No. DE-AC02-05CH11231, and the resources of the Texas Advanced Computing Center (TACC), Austin, Texas.

*akr@uta.edu

[1] J. J. Katz, G. T. Seaborg, and L. R. Morss, *The Chemistry of the Actinide Elements* (Chapman and Hall, London, 1986).
[2] *Transuranium Elements: A Half Century*, edited by L. R. Morss and J. Fuger (American Chemical Society, Washington, D.C., 1992).
[3] *The Chemistry of the Actinide and Transactinide Elements*, edited by L. R. Morss, N. M. Edelstein, J. Fuger, and J. J. Katz (Springer, New York, 2006), Vols. 1–5.
[4] *Actinides: Basic Science, Applications, and Technology*, edited by L. Soderholm, J. J. Joyce, M. F. Nicol, D. K. Shuh, and J. G. Tobin, MRS Symposia Proceedings No. 802 (Materials Research Society, Pittsburgh, 2004).
[5] *Actinides 2005—Basic Science, Applications, and Technology*, edited by J. L. Sarrao, A. J. Schwartz, M. R. Antonio, P. C. Burns, R. G. Haire, and H. Nitsche, MRS Symposia Proceedings No. 893 (Materials Research Society, Pittsburgh, 2005).
[6] *Actinides 2006—Basic Science, Applications, and Technology*, edited by K. J. M. Blobaum, E. A. Chandler, L. Havela, M. B. Maple, and M. P. Neu, MRS Symposia Proceedings No. 986 (Materials Research Society, Pittsburgh, 2006).
[7] P. Söderlind, O. Eriksson, B. Johansson, J. M. Wills, and A. M. Boring, Nature (London) **374**, 524 (1995).
[8] N. M. Edelstein, B. Johansson, and J. L. Smith, in *Opportunities and Challenges in Research with Transplutonium Elements* (National Academy Press, Washington, D.C., 1983), p. 299.
[9] *Plutonium Futures: The Science*, edited by K. S. Pillay and K. C. Kim, AIP Conf. Proc. No. 532 (AIP, Melville, NY, 2000).
[10] *Plutonium Futures: The Science*, edited by G. D. Jarvinen, AIP Conf. Proc. No. 673 (AIP, Melville, NY, 2003).
[11] A. M. Boring and J. L. Smith, in Challenges in Plutonium Science, special issue of Los Alamos Sci. **1**, 90 (2000).
[12] *Advances in Plutonium Chemistry 1967–2000*, edited by D. Hoffman (American Nuclear Society, La Grange Park, IL/University Research Alliance, Amarillo, TX, 2002).
[13] *Plutonium Handbook, A Guide to the Technology*, edited by O. J. Wick (American Nuclear Society, Lagrange Park, IL, 1980), Vol. 1.
[14] D. A. Young, *Phase Diagrams of the Elements* (University of California Press, Berkeley, 1991).
[15] W. H. Zachariasen and F. H. Ellinger, Acta Crystallogr. **16**, 777 (1963).
[16] A. C. Lawson, B. Martinez, J. A. Roberts, B. I. Bennet, and J. W. Richardson, Jr., Philos. Mag. B **80**, 53 (2000).
[17] S. Y. Savrasov, G. Kotliar, and E. Abrahams, Nature (London) **410**, 793 (2001).
[18] P. Söderlind, J. M. Wills, B. Johansson, and O. Eriksson, Phys. Rev. B **55**, 1997 (1997).
[19] A. V. Postnikov and V. P. Antropov, Comput. Mater. Sci. **17**, 438 (2000).
[20] O. Eriksson, L. E. Cox, B. R. Cooper, J. M. Wills, G. W. Fernando, Y.-G. Hao, and A. M. Boring, Phys. Rev. B **46**, 13576 (1992).
[21] J. van Ek, P. A. Sterne, and A. Gonis, Phys. Rev. B **48**, 16280 (1993).
[22] A. O. Shorikov, A. V. Lukoyanov, M. A. Korotin, and V. I. Anisimov, Phys. Rev. B **72**, 024458 (2005).
[23] J. Bouchet, R. C. Albers, M. D. Jones, and G. Jomard, Phys. Rev. Lett. **92**, 095503 (2004).
[24] F. J. Espinosa, P. Villela, J. C. Lashley, S. D. Conradson, L. E. Cox, R. Martinez, B. Martinez, L. Morales, J. Terry, and R. A. Pereyra, Phys. Rev. B, **63**, 174111 (2001).
[25] J. Kollár, L. Vitos, and H. L. Skriver, Phys. Rev. B **55**, 15353 (1997).
[26] D. C. Wallace, Phys. Rev. B **58**, 15433 (1998).
[27] M. I. Baskes, Phys. Rev. B **62**, 15532 (2000).
[28] A. J. Arko, J. J. Joyce, L. Morales, J. Wills, J. Lashley, F. Wastin, and J. Rebizant, Phys. Rev. B **62**, 1773 (2000); A. J. Arko, J. J. Joyce, and L. Morales, J. Alloys Compd. **286**, 14 (1999).
[29] M. Pénicaud, J. Phys.: Condens. Matter **12**, 5819 (2000); **14**, 3575 (2002).
[30] L. Havela, T. Gouder, F. Wastin, and J. Rebizant, Phys. Rev. B **65**, 235118 (2002); T. Gouder, L. Havela, F. Wastin, and J. Rebizant, Europhys. Lett. **55**, 705 (2001); T. Gouder, J. Electron Spectrosc. Relat. Phenom. **101-103**, 419 (1999).
[31] J. C. Lashley, A. Lawson, R. J. McQueeney, and G. H. Lander, Phys. Rev. B **72**, 054416 (2005).
[32] B. Sadigh, P. Söderlind, and W. G. Wolfer, Phys. Rev. B **68**, 241101(R) (2003); P. Söderlind, Europhys. Lett. **55**, 525 (2001).
[33] M. Robert, A. Pasturel, and B. Siberchicot, J. Phys.: Condens. Matter **15**, 8377 (2003).
[34] A. L. Kutepov and S. G. Kutepova, J. Phys.: Condens. Matter **15**, 2607 (2003).
[35] H. R. Gong and A. K. Ray (unpublished).
[36] R. Atta-Fynn and A. K. Ray, Phys. Rev. B **75**, 195112 (2007); Physica B **392**, 112 (2007); **400**, 307 (2007).
[37] J. P. Perdew, K. Burke, and M. Ernzerhof, Phys. Rev. Lett. **77**, 3865 (1996).
[38] P. Blaha, K. Schwarz, G. K. H. Madsen, D. Kvasnicka, and J. Luitz, computer code WIEN2K (Vienna University of Technology, Austria, 2001).
[39] G. K. H. Madsen, P. Blaha, K. Schwarz, E. Sjöstedt, and L. Nordström, Phys. Rev. B **64**, 195134 (2001).
[40] F. Wagner, Th. Laloyaux, and M. Scheffler, Phys. Rev. B **57**, 2102 (1998).
[41] D. D. Koelling and B. N. Harmon, J. Phys. C **10**, 3107 (1977).
[42] J. Kunes, P. Novak, R. Schmid, P. Blaha, and K. Schwarz, Phys. Rev. B **64**, 153102 (2001).
[43] A. K. Ray and J. C. Boettger, Phys. Rev. B **70**, 085418 (2004); Int. J. Quantum Chem. **105**, 564 (2005); H. R. Gong and A. K. Ray, Eur. Phys. J. B **48**, 409 (2005); Surf. Sci. **600**, 2231 (2006); D. Gao and A. K. Ray, *ibid.* **600**, 4941 (2006).
[44] A. Soon, M. Todorova, B. Delley, and C. Stampfl, Phys. Rev. B **73**, 165424 (2006).
[45] A. Kokalj, J. Mol. Graphics Modell. **17**, 176 (1999); code available from http://www.xcrysden.org